Role of the *X* minimum in transport through AlAs single-barrier structures

J. J. Finley*
Department of Physics, University of Sheffield, Sheffield, S3 7RH, United Kingdom

R. J. Teissier
Laboratoire de Microstructures et Microélectronique, 196 Avenue Henri Ravera, Bagneux Cedex 92555, France

M. S. Skolnick, J. W. Cockburn, and G. A. Roberts
Department of Physics, University of Sheffield, Sheffield, S3 7RH, United Kingdom

R. Grey, G. Hill, and M. A. Pate
EPSRC Central Facility, Department of Electronic and Electrical Engineering, University of Sheffield, Sheffield, S1 3JD, United Kingdom

R. Planel
Laboratoire de Microstructures et Microélectronique, 196 Avenue Henri Ravera, Bagneux Cedex 92555, France
(Received 23 February 1998; revised manuscript received 22 June 1998)

We report an electrical transport and electroluminescence (EL) spectroscopy study of single-barrier GaAs-AlAs-GaAs *p-i-n* tunnel structures with a barrier thickness in the range 4.5–8.0 nm. The results permit us to determine directly the relative roles of nonresonant Γ-Γ tunneling and resonant Γ-*X*-Γ intervalley transfer in the transport through the indirect-gap tunnel barriers. The Γ-*X*-Γ transport is shown to take place predominantly without conservation of transverse wave vector ($k_\parallel$), with $k_\parallel$-conserving scattering via X_z states only significantly close to the onset of Γ-*X* intervalley transfer. By detecting extremely weak EL arising from excited X_z states we show that the complete Γ-*X*-Γ transport process is very strongly sequential and determine, quantitatively, the comparative time scales for *X*-Γ and inter-*X*-level scattering. The bias-dependent Γ-*X*-Γ and Γ-Γ transport times are determined for AlAs barrier widths in the range 3.0–10 nm. The intervalley Γ-*X*-Γ transport model yields results in good agreement with experiment and demonstrates that, providing intervalley Γ-*X* transfer is energetically possible, nonresonant Γ-Γ tunneling only contributes significantly to the transport characteristics for barrier widths of ~3 nm or less. [S0163-1829(98)04540-8]

I. INTRODUCTION

Over the past few years there has been widespread interest in the nature of electron transport processes through GaAs-AlAs-GaAs heterostructures. This has arisen from both the numerous device applications of such structures and the potential for studying novel transport phenomena in this materials system. Mendez *et al.*,[1] were the first workers to draw attention to the possibility of multiband transport processes in GaAs-AlAs heterostructures involving conduction-band states in the AlAs layer with different symmetry and location in wave-vector (k) space. GaAs has a direct band gap with the lowest conduction-band minimum lying at the Γ($\mathbf{k}=\mathbf{0}$) point of the Brillouin zone. By contrast, AlAs has an indirect band gap with conduction-band minima close to or at the *X* point [001].[2,3] Electron transport through GaAs-AlAs-GaAs single-barrier structures may thus arise either from nonresonant tunneling through the AlAs barrier (Γ-Γ tunneling) or from intervalley transfer via quasilocalized *X* states in the barrier (Γ-*X*-Γ transport).

Previously we have reported the determination of the Γ-*X* (emitter-barrier) intervalley transfer mechanisms in GaAs-AlAs heterostructures by modelling of the electrical transport characteristics.[4] Clear features were identified in the conductance-voltage (σ-V) curves arising from transfer via *X*-point conduction-band minima both parallel (X_z) *and* perpendicular (X_{xy}) to the direction of current flow. In contrast with previous works[5–9] both X_z and X_{xy} states were shown to be strongly involved in the Γ-*X*-Γ transport process, with Γ-X_{xy} scattering being predominantly inelastic while transfer via X_z states was shown to take place elastically. Inelastic transfer via X_{xy} is expected to proceed without conservation of the transverse wave vector ($k_\parallel$) since the transverse *X* minima lie close to the Brillouin zone boundary in the k_x and k_y directions. By contrast, the X_z minima lie close to $k_\parallel=0$ and Γ-X_z intervalley transfer can proceed both with ($\Delta k_\parallel=0$) and without ($\Delta k_\parallel\neq 0$) conservation of $k_\parallel$.

Although significant advances were achieved in Ref. 4, we focus here on several other important aspects of Γ-*X* transfer. In particular we direct attention to sharp features in σ-V observed close to the onset of Γ-X_z transfer, we report the observation and analysis of excited X_z state electroluminescence transitions and present a combined theoretical/experimental analysis of a key aspect of transport through AlAs barriers, namely, the relative roles of Γ-*X*-Γ and Γ-Γ channels as a function of barrier width.

We begin the present paper by presenting a qualitative discussion of the form of the I-V and σ-V characteristics expected for Γ-*X* intervalley transfer, proceeding either with or without $k_\parallel$ conservation. This discussion provides the ba-

sis for a sound physical understanding of the detailed shapes of the features observed in the transport characteristics. We then explain why $k_\parallel$ nonconserving processes dominate resonant transfer via X_z states, whereas they play a much less significant role in other more widely investigated (Γ-Γ-Γ) resonant tunneling systems such as GaAs-$Al_xGa_{1-x}As$ ($x<0.4$) double-barrier tunneling devices. The $k_\parallel$ nonconserving transfer model[4] accounts very well for nearly all the features observed in the σ-V characteristics for all samples investigated. However, the sharp features in σ-V we report for barrier widths of 6 nm and less are shown to arise from a weak $\Delta k_\parallel = 0$ Γ-X_z conduction channel. Such Γ-X_z-Γ processes were assumed in much previous work to dominate the Γ-X-Γ intervalley transport.[5–9]

Study of the electroluminescence (EL) from the p-i-n diodes provides complementary information on the comparative roles of the Γ-X-Γ and Γ-Γ transport channels. For barrier widths of 6 nm and less, a pronounced transition is observed, with increasing device bias, which reflects directly the transition from nonresonant Γ-Γ tunneling to resonant Γ-X-Γ transfer. By detecting extremely weak high energy EL arising from electrons populating *excited* X_z states, comparative estimates of both the intervalley Γ-X and X-Γ transfer times, and the inter X-level relaxation time, are obtained.

Finally, quantitative values for the Γ-X-Γ transfer time are calculated as a function of electric field for various AlAs barrier widths in the range 3.0–10 nm. By comparing these results with calculated Γ-Γ tunneling times we show that the Γ-X-Γ channel *dominates* electron transport in GaAs-AlAs-GaAs structures, *whenever* Γ-X intervalley transfer is energetically possible. This conclusion is shown to be valid for barrier widths down to ~3 nm, with nonresonant Γ-Γ channels only dominating for barrier widths less than ~2.5 nm.

The paper is organized as follows: in Sec. II the experimental details are summarized. This is followed in Sec. III by the qualitative discussion of the expected form of Γ-X-Γ transport characteristics. The I-V and σ-V results then follow in Sec. IV and are compared with these qualitative expectations. Electroluminescence spectra from both ground and excited X states are presented in Secs. V and VI with calculations of Γ-Γ and Γ-X-Γ transport times following in Sec. VII. Finally, the conclusions are summarized in Sec. VIII.

II. EXPERIMENTAL DETAILS

The experiments were carried out on three p-i-n GaAs-AlAs-GaAs single-barrier heterostructures, grown by molecular beam epitaxy in two different laboratories. The structures studied consisted of the following layers grown on n^+-type GaAs substrates: 0.5-μm $n=2\times10^{18}$-cm^{-3} GaAs buffer layer, 50-nm $n=1\times10^{17}$-cm^{-3} GaAs, 50-nm $n=3\times10^{16}$-cm^{-3} GaAs emitter, 5-nm undoped GaAs spacer, 4.5 nm, 6 nm or 8 nm undoped AlAs barrier, 5-nm undoped GaAs spacer, 0.5-μm $p=1\times10^{17}$-cm^{-3} GaAs collector and 0.5-μm $p=1\times10^{18}$-cm^{-3} GaAs top contact. The samples were processed into 200-μm-diameter circular mesa structures with annular top contacts to facilitate optical access. Electroluminescence was collected by an *in situ* fiber optic system, dispersed by a triple-grating spectrometer and detected by a high sensitivity N_2-cooled Si charge-coupled device detector array. For measurements at both zero and finite magnetic field the samples were maintained at a stabilized temperature of 1.7 K in the vertical bore of a 16 T superconducting magnet.

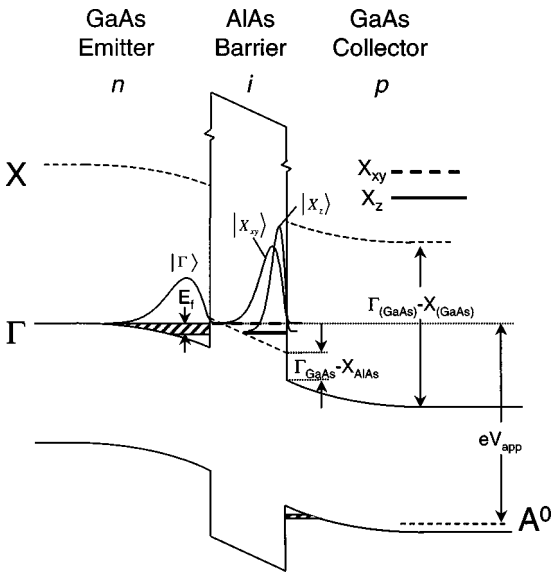

FIG. 1. Schematic representation of the band structure of the p-i-n GaAs/AlAs/GaAs tunnel diodes investigated. The conduction-band minima at the Γ and X points of the Brillouin zone are shown by the full and dashed lines, respectively. The X point potential forms a quantum well within the AlAs barrier, with the Γ-X transfer process then taking place between the Γ-symmetry 2D emitter states and quasilocalized X states within the AlAs barrier. Schematic envelope functions for the Γ (emitter) and a single X_z (longitudinal) and X_{xy} (transverse) state are shown.

III. ELECTRON TRANSPORT MECHANISMS THROUGH GaAs-AlAs-GaAs STRUCTURES: QUALITATIVE DISCUSSION

A schematic band diagram of the structures under applied forward bias is shown in Fig 1. The zone center (Γ) and zone boundary (X) conduction-band profiles are shown by full and dashed lines, respectively. Since the Γ(GaAs)-X(AlAs) conduction-band offset is significantly less than the X(GaAs)-Γ(GaAs) separation, a quantum well for electrons is formed at the X point of the Brillouin zone within the AlAs ''barrier.'' Within this X-point quantum well both the longitudinal (X_z) and transverse (X_{xy}) X minima give rise to quasiconfined states.[10] The ordering of these X states is determined by the competing effects of quantum confinement and strain[11] with the result that for AlAs layer thicknesses less than ~7 nm the lowest state has X_z symmetry, while for greater layer thicknesses the lowest states are X_{xy}-like.[12]

For applied forward biases (V_{app}) greater than the built-in voltage of the p-i-n junction (~1.5 V), two-dimensional (2D) electron and hole accumulation layers are formed on either side of the AlAs barrier. In our structures, the low doping concentration in this region ensures that the accumulation layer states are two dimensional (2D) in nature. Electron and/or hole tunneling then occurs from these accumulation layers through the AlAs barrier with minority carriers

injected into the *p* and/or *n* regions, respectively. The energy separation between the Fermi level of the 2D electron accumulation layer and the confined *X* states within the barrier may be accurately controlled by adjusting $V_{\rm app}$.

We now discuss the qualitative form of the *I*-*V* and σ-*V* characteristics expected for Γ-*X*-Γ transport through the AlAs tunnel barrier. The discussion provides the basis for understanding the form of the σ-*V* results in Sec. IV and illustrates the principal differences between such resonant transfer via *X* states and the more familiar case of resonant (Γ-Γ-Γ) tunneling in GaAs-$Al_xGa_{(1-x)}As$ double-barrier heterostructures. These differences arise primarily as a consequence of the differing effective masses of the Γ and *X* states between which transport occurs in the Γ-*X*-Γ case, in contrast with Γ-Γ-Γ resonant tunneling where the effective masses of all states involved are very similar.

The Γ-*X*-Γ transport involves two intervalley transfer steps, firstly across the emitter (GaAs)-barrier (AlAs) interface [Γ(GaAs)-*X*(AlAs)], followed by a further *X*(AlAs)-Γ(GaAs) transfer at the barrier-collector interface. The rate for such Γ-*X* transfer is well described by an expression of the form[13]

$$\frac{1}{\tau_{\Gamma X}} = |\langle \Gamma | X \rangle|^2 P^0, \tag{1}$$

where $|\Gamma\rangle$ and $|X\rangle$ represent the normalized envelope functions describing the Γ and *X* states involved and P^0 is an intrinsic rate for $\Gamma \rightarrow X$ transfer.[4] A similar expression applies also to the $X \rightarrow \Gamma$ transfer. In Γ-*X*-Γ transport, the electric field in the AlAs barrier results in the *X*-state envelope functions being strongly localized close to the AlAs (barrier)-GaAs(collector) interface as shown schematically on Fig. 1. This enhances the *X*(barrier)-Γ(collector) envelope function overlap [Eq. (1)] and consequently the Γ(emitter) $\rightarrow$*X*(barrier) transfer step is expected to govern the form of the *I*-*V* and σ-*V* characteristics.[4]

The degree to which in-plane wave vector ($k_\parallel$) is conserved in $\Gamma \rightarrow X$ transfer has a strong influence on the form of the Γ-*X*-Γ current expected. We first consider the situation for $\Gamma \rightarrow X$ transfer without $k_\parallel$ conservation ($\Delta k_\parallel \neq 0$) followed by the case with $k_\parallel$ conservation ($\Delta k_\parallel = 0$), although in reality, which mechanism dominates depends on the symmetry of the *X* states involved and the degree of residual disorder in the system.

Energy versus in-plane wave-vector (E-$k_\parallel$) dispersion relations for the Γ emitter states and a single *X* barrier subband are shown in Fig. 2 for four values of $V_{\rm app}$ (V_a, V_b, V_c, and V_d). These values correspond to the situations where the Γ and *X* 2D subband minima are separated by energies $\Delta E = E_f$ (V_a), $0 \leqslant \Delta E \leqslant E_f$ (V_b, V_c), $\Delta E = 0$ (V_d), where E_f is the bias-dependent Fermi energy of the populated emitter states represented by the heavy curve on the figure. The open (filled) circles correspond to populated emitter states, which may participate in $\Delta k_\parallel \neq 0$ ($\Delta k_\parallel = 0$) transfer while simultaneously satisfying energy (and $k_\parallel$) conservation requirements.

A. $k_\parallel$ nonconserving Γ-*X* transfer

Figure 2(b) shows a schematic representation of the *I*-*V* (full lines) and σ-*V* (dashed lines) variation expected for Γ

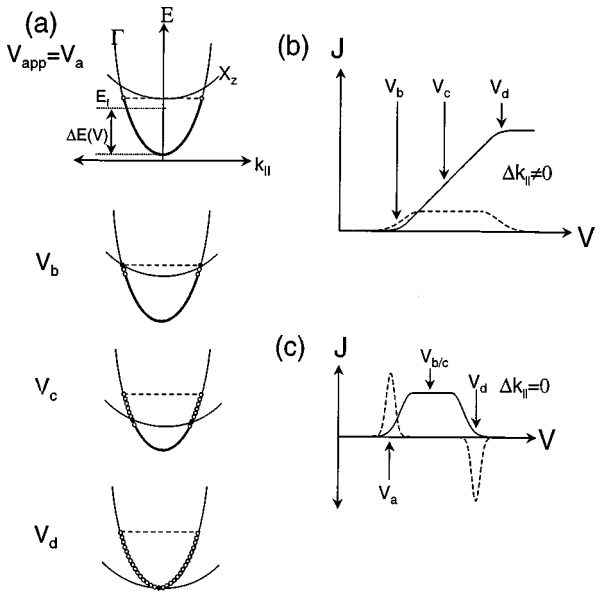

FIG. 2. (a) Γ and *X* subbands depicted in E-$k_\parallel$ space for Γ-*X* transfer proceeding with (●) or without (○) conservation of the transverse wave vector ($k_\parallel$) for four values of the applied bias. Also shown are the schematic forms expected for the current-voltage (*I*-*V*) and differential conductance–voltage (σ-*V*) characteristics when tunneling via a single, isolated, *X* state is considered. The two sets of curves in (c) and (b), respectively correspond to Γ-*X* transfer with and without conservation of the transverse wave vector.

electrons transferring through a *single X* subband *without* $k_\parallel$ conservation. Additional effects due to changes in the strength of the Γ-*X* coupling [Eq. (1)] and the variation of E_f with $V_{\rm app}$ are not included in the present qualitative discussion. Increasing $V_{\rm app}$ results in the energy of the *X* states within the barrier being lowered relative to the Γ (emitter) states. Intervalley Γ-*X* transfer first becomes possible at a bias such that the lowest *X* subband in the AlAs layer becomes resonant with populated emitter states close to the Fermi energy [$V_{\rm app} = V_a$, Fig. 2(a)]. Further increase of $V_{\rm app}$ leads to a linear increase of *I*, since the number of electron states from which intervalley transfer can occur [shown by the open circles in Fig. 2(a)] increases linearly with bias, reflecting the 2D emitter density of states. As $V_{\rm app}$ increases beyond V_c, when the bottom of the *X* subband moves below the bottom of the Γ subband, no further increase in *I* can occur and the current saturates [full line, Fig. 2(b)]. The corresponding σ-*V* variation, shown by a dashed line in the figure, is a broadened step function with a width determined by E_f and an amplitude proportional to the strength of the coupling between Γ and *X* states.[4]

When the emitter Fermi energy is greater than the separation between *X* subbands, as is the case for our structures, the resonances in σ-*V* are expected to be strongly overlapping, with transfer into more highly excited subbands commencing before the cutoff of transport into the previous subband. Thus, we expect the overall σ-*V* variation for $\Delta k_\parallel \neq 0$ Γ-*X*-Γ transfer to consist of a series of steplike increases, each step corresponding to the opening of another Γ-*X* transfer channel. We note that $\Delta k_\parallel \neq 0$ transfer may involve either X_z or X_{xy} states while $k_\parallel$-conserving transfer (described below) involves only X_z states that lie close to $k_\parallel = 0$.

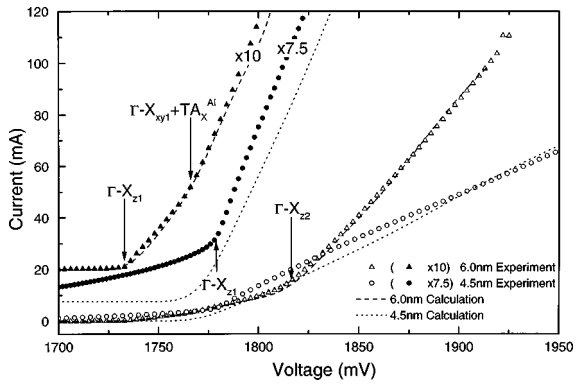

FIG. 3. *I-V* characteristics of 4.5 (circles) and 6.0 nm (triangles) barrier samples measured at $T=1.7$ K. The dashed (dotted) lines on the figure show the calculated *I-V* characteristics for the 4.5-nm (6-nm) samples obtained using the Γ-*X*-Γ transport model described in the text.

B. $k_\parallel$-conserving Γ-*X* transfer

For Γ-*X*-Γ transport with conservation of in-plane wave vector, the onset of intervalley transfer arises at a bias $V_{\rm app}=V_b$ where energy *and* transverse momentum ($k_\parallel$) can first be conserved between populated Γ emitter and X_z barrier states. In contrast to the $\Delta k_\parallel\neq 0$ case, the number of states from which intervalley transfer can occur is now bias *independent* [filled circles, Fig. 2(a)] until the cutoff of the resonance is reached when the minima of the Γ and empty X_z subbands are aligned. The resulting *I-V* curve is thus expected to adopt a steplike form, as shown by the full curve in Fig. 2(c), with the corresponding σ-*V* curve showing positive- and negative-going peaks at the onset and cutoff of the resonance, respectively (dashed lines in the figure). The broadening of the resonance in *I-V* is proportional to a factor $E_f(1-m_\Gamma^*/m_X^*)$, which arises directly from the effective-mass difference between the emitter Γ and X_z states.

The *I-V* characteristics expected for $\Delta k_\parallel=0$ Γ-X_z-Γ resonant transfer (2D-2D) thus contrast strongly with the more familiar case of $\Delta k_\parallel=0$ Γ-Γ-Γ resonant tunneling (2D-2D). In the latter case, the effective masses of the emitter and quantum well states are the same, and energy and $k_\parallel$ are only conserved at a single value of $V_{\rm app}$ for the *entire* emitter distribution. As a result, strongly peaked structure is predicted theoretically and observed experimentally in *I-V*. The situation when the effective mass characterizing the quantum well and contact regions differ has been considered by Ohno *et al.*[14] for 3D-2D resonant tunneling. In this work, the additional degree of freedom in the 3D contact was shown to result mainly in a distortion of the shape of the resonance with the majority of emitter electrons still able to participate in $\Delta k_\parallel=0$ transport. By contrast, in the present case only a very small fraction of populated emitter states are available to participate in $\Delta k_\parallel=0$ transfer over the width ($V_b<V_{\rm app}<V_d$) of the resonance. Thus, we expect that $\Delta k_\parallel\neq 0$ processes will contribute much more strongly than for Γ-Γ-Γ resonant tunneling where they play only a minor role.

IV. ELECTRICAL TRANSPORT: EXPERIMENTAL RESULTS AND DISCUSSION

Figures 3 and 4 show the *I-V* and σ-*V* characteristics of

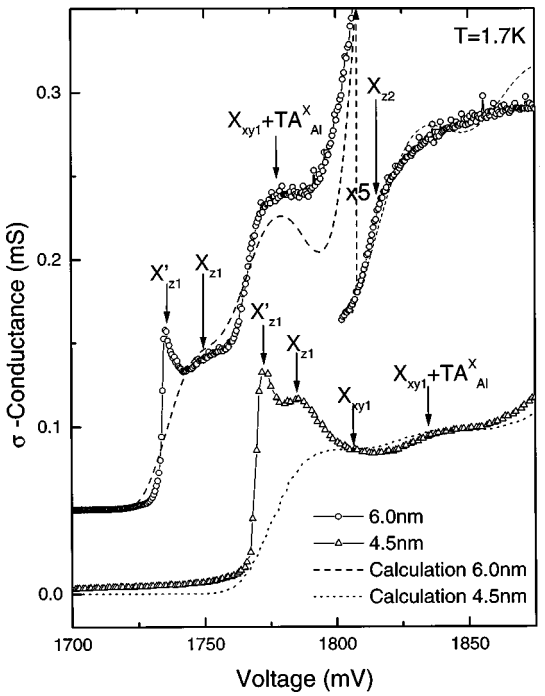

FIG. 4. Experimental and calculated σ-*V* curves for the 4.5- and 6-nm samples measured at $T=1.7$ K. The dashed (dotted) lines on the figure show the calculated σ-*V* characteristics for the 4.5-nm (6-nm) samples, including elastic/inelastic Γ-X_z and Γ-X_{xy} transfer processes. The onsets of the resonant features are labeled by the index of the *X* state (and phonon) involved.

the 4.5-nm and 6-nm barrier samples measured at 1.7 K. For both samples, current flow begins at an applied bias close to ~1500 mV corresponding to the built-in potential of the *p-i-n* tunnel diodes. The current then increases smoothly for voltages less than ~1700 mV before increasing sharply at a barrier-width-dependent threshold marked by arrows in the figure. We identify the smoothly increasing current, at low bias, as arising from nonresonant Γ-point tunneling of electrons[15] through the AlAs barrier. As expected, the magnitude of such nonresonant tunneling current decreases strongly with increasing barrier width, reflecting the decrease of the nonresonant tunneling probability. The sharp increases of the current correspond to the onset of Γ-*X* intervalley transfer with additional onsets observed at higher biases (marked by arrows in Fig. 3) corresponding to the opening of successive overlapping Γ-*X* transport channels. Devices with wider barriers (up to 10 nm) exhibit qualitatively similar, although more complex, behavior to the 6.0- and 4.5-nm barrier samples discussed here.[4]

The resonant features of Fig. 3 are more easily visualized in the σ-*V* curves of Fig. 4, which consist of a series of overlapping step and peaklike increases. Most of the features observed in Figs. 3 and 4 are consistent with the expectations of Sec. III for $\Delta k_\parallel\neq 0$ Γ-*X* transfer [Fig. 2(b)]. These similarities are particularly evident for the 6-nm sample, which exhibits three clear conductance steps at 1730, 1770, and 1810 mV. As anticipated in Sec. III, negative differential resistance features as associated with $\Delta k_\parallel=0$ Γ-Γ-Γ resonant tunneling are not observed. Accurate identification of the features in Figs. 3 and 4 was obtained by self-consistent solution of Poisson and Schrödinger equations within the

envelope function approximation. The most important input is a reliable knowledge of the variation of the electric field across the emitter/barrier region as a function of $V_{\rm app}$ and was obtained from Shubnikov–de Haas–like magnetotransport (I-B) measurements.[16]

With a knowledge of the variation of electric field with bias, the I-V and σ-V characteristics were calculated, assuming full relaxation of the requirements for $k_\parallel$ conservation. With the assumption of $\Delta k_\parallel \neq 0$ transfer, the current density flowing through the ith$X$ subband is given by $J_i = eN_s/\tau_{\Gamma X}$. $\tau_{\Gamma X}$ is calculated from Eq. (1) for each X state, N_s is the emitter density, which may transfer into the X state, satisfying energy conservation [$N_s \approx (\Delta E/E_f) n_s$], and ΔE is the energy separation between the emitter Fermi level and the X state (Fig. 2). The total X channel current is then calculated by summing over all X states available for conduction.

The dashed and dotted lines in Figs. 3 and 4 show the results of the calculation for the 4.5- and 6.0-nm samples. It is seen that the $k_\parallel$ nonconserving model accurately reproduces the general form and onset positions of nearly all the observed features. In addition, the calculation confirms the identification of the current onsets in I-V observed at 1775 mV (4.5 nm) and 1735 mV (6 nm) as corresponding to the onset of Γ-X transfer. The parameters were identical to those used in Ref. 4 for 6-, 8-, and 10-nm barrier samples. It is notable that the cutoffs of the resonances, expected both for the $\Delta k_\parallel \neq 0$ or $\Delta k_\parallel = 0$ models [Figs. 2(b) and 2(d)] are not observed. As anticipated in Sec. III, this behavior has a very natural explanation since the typical Fermi energy of the populated Γ emitter states ($E_f \sim 25-40$ meV) is greater than the energy separation between resonances. Individual resonances are, therefore, strongly overlapping with the opening of the next X channel occurring before the cutoff of the previous resonance. The possibility for multiple, overlapping resonances at a single $V_{\rm app}$ contrasts strongly with Γ-Γ-Γ resonant tunneling in which transport proceeds via a single quantum state at any specific value of $V_{\rm app}$.

The assumption of nonconservation of $k_\parallel$ is expected to hold well for the X_{xy} resonances, since they require a large change of $k_\parallel$. However, the accuracy of the assumption is less clear for Γ-X_z transfer. Indeed, in magnetotransport measurements,[17] we have found evidence for an increasing contribution from $\Delta k_\parallel = 0$ Γ-X_z transfer processes at elevated magnetic field.

Closer examination of the Γ-X_{z1} resonance for the 4.5-nm sample in Fig. 4 shows there is a sharp peak in σ-V close to the onset of Γ-X transfer (X'_{z1} at $V_{\rm app} \sim 1780$ mV). A similar sharp onset peak is also observed for the 6.0-nm barrier sample ($\sim$1735 mV) in which the first resonance encountered also arises from elastic Γ-X_{z1} transfer. Such sharply peaked structure is consistent with the qualitative expectations for $\Delta k_\parallel = 0$ elastic transfer [see Fig. 2(c) and discussion of Sec. III B] and cannot be reproduced by the $\Delta k_\parallel \neq 0$ model [Fig. 2(b)].

It is notable that $\Delta k_\parallel = 0$-like structure is only observed at biases close to onset where the strongest contribution to σ arises from Γ-X_{z1} transfer. Under these conditions, only emitter electrons close to the Fermi level may undergo Γ-X_{z1} elastic transfer, with similar numbers available to participate in either $\Delta k_\parallel = 0$ and $\Delta k_\parallel \neq 0$ transitions [see Fig. 2(a), $V_{\rm app} = V_b$]. Thus, $\Delta k_\parallel = 0$ Γ-X_{z1} transfer may be observed close to onset, since it is expected to be an intrinsically much stronger process *per emitter electron* than disorder-induced ($\Delta k_\parallel \neq 0$) elastic transfer.[18] However, as $V_{\rm app}$ is increased beyond the onset of Γ-X transfer, a rapidly increasing number of emitter electrons can access $\Delta k_\parallel \neq 0$ Γ-X transfer channels (see Fig. 4) and the comparatively weak $\Delta k_\parallel = 0$ component becomes submerged in the broader conductance signal arising from $\Delta k_\parallel \neq 0$ processes. Thus $\Delta k_\parallel = 0$ features are only expected to be observed close to the initial onset of Γ-X-Γ conductance. This interpretation is supported by the form of the σ-V characteristics obtained from wider barrier samples (see Ref. 4). In such devices, similar sharply peaked structure is absent since the strongest contribution to σ close to onset arises from elastic Γ-X_{xy1} transfer where, as described above, $\Delta k_\parallel = 0$ transfer may not occur.

Finally in this section we note that the good quantitative fits obtained to both I-V and σ-V over a wide range of bias indicate that nonresonant Γ-Γ tunneling provides a negligible contribution to the total current for $V_{\rm app}$ beyond the onset of Γ-X transfer. This conclusion is confirmed by the EL measurements and supported by the calculations in Secs. VI and VII.

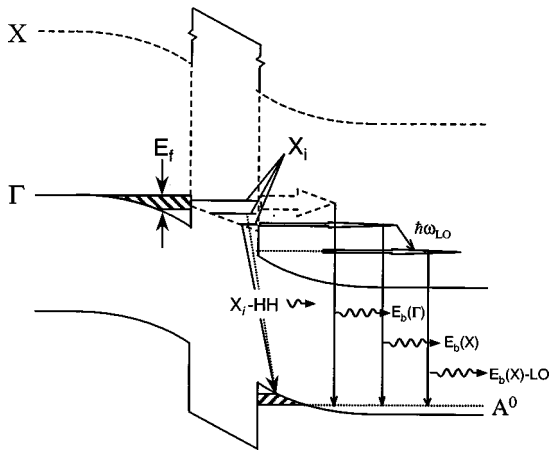

FIG. 5. Schematic band-edge diagram showing the main processes leading to the generation of high-energy type-II and hot-electron EL in the p-i-n structures investigated.

V. ELECTROLUMINESCENCE SPECTROSCOPY

Figure 5 shows the main processes leading to the generation of high energy EL in the devices investigated. For biases below the threshold for intervalley Γ-X transfer ($V_{\rm app} < 1700$ mV) a population of hot electrons is injected into the p-type collector by nonresonant Γ-Γ tunneling through the AlAs barrier. These highly energetic electrons then relax by sequential emission of zone center LO phonons ($\hbar\Omega_{\rm LO} \sim 36$ meV), generating EL by recombining with holes localized at Be acceptors[19,20] (e-A^0 recombination). Such hot electron EL is expected to be qualitatively similar to that observed from direct gap GaAs-$Al_xGa_{(1-x)}As$-GaAs p-i-n structures,[21] consisting of a broad bias-dependent peak arising from the recombination of ballistic electrons [$E_b(\Gamma)$], together with a number of LO phonon satellites

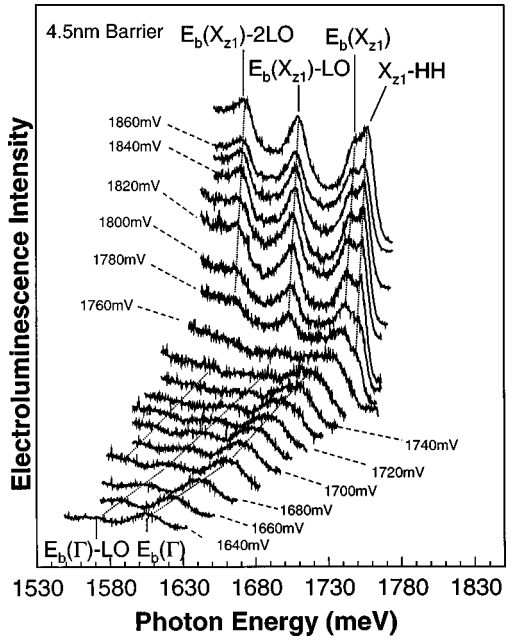

FIG. 6. Low temperature ($T=1.7$ K) EL spectra obtained from the 4.5-nm barrier sample as a function of the applied bias. The low bias ($V_{\rm app}<1760$ mV) EL spectra are very weak and exhibit qualitatively similar features to those observed in tunneling through direct-gap single barrier structures. At higher bias, a pronounced change in form is observed with a sudden enhancement of the spectral resolution together with a dramatic decrease in the peak shift rate with applied bias. Features corresponding to both Γ-Γ [$E_b(\Gamma) - iLO$] and Γ-X-Γ [$X_{z1}-HH$ and $E_b(X_{z1})-iLO$] transport of electrons through the AlAs tunnel barrier are observed.

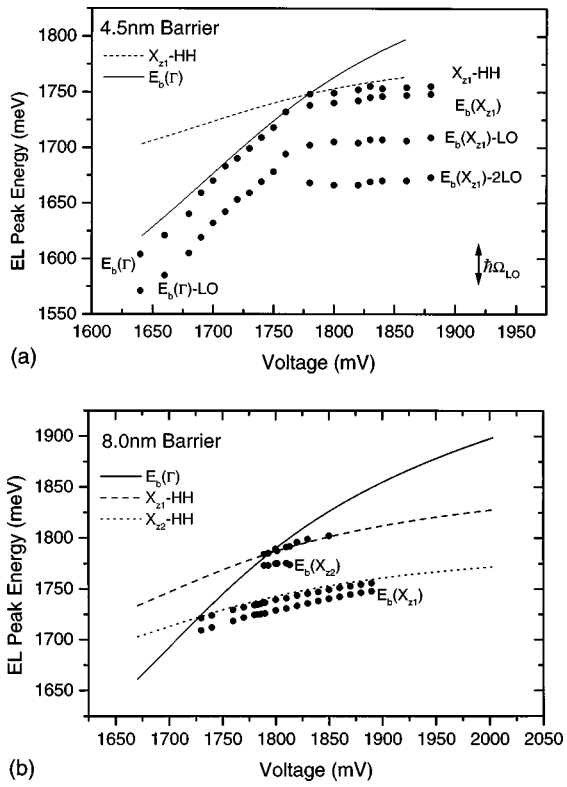

FIG. 7. EL peak positions for 4.5-nm (a) and 8.0-nm (b) barrier samples. The full (dashed) lines show the calculated energy at which $E_b(\Gamma)$ ($X_{z1}-HH$) EL emission is expected to arise.

[$E_b(\Gamma)$-iLO] at multiples of $\hbar\Omega_{\rm LO}$ to lower energy. For biases beyond the threshold for Γ-X transfer, electrons are also injected into the collector from X states within the AlAs barrier. This produces additional hot-electron EL cascades that reflect the distribution of X-point electrons in the AlAs barrier [$E_b(X)$-iLO, $i=0,1,\ldots$]. We expect the relative strengths of the ballistic $E_b(\Gamma)$ and $E_b(X)$ EL peaks to provide a quantitative comparison of the roles of nonresonant Γ-Γ and resonant Γ-X-Γ transport processes. In addition to hot-electron EL, X_z electrons in the barrier generate EL arising from zero-phonon type-II recombination[22] with holes localized close to the barrier on the p side (X_i-HH, Fig. 5).

Figure 6 shows EL spectra obtained from the 4.5-nm sample for biases from 1640 to 1860 meV. The energies of the EL peaks are plotted as a function of $V_{\rm app}$ in Fig. 7(a). It is seen that the highest-energy peak arises at an energy very close to $eV_{\rm app}$ for $V_{\rm app}<1775$ mV, the voltage at which Γ-X intervalley transfer commences [see Figs. 3 and 4].[23] The $E_b(\Gamma)$ identification is confirmed by calculations of the energy expected for such ballistic EL from the self-consistent Poisson-Schrödinger modeling of Sec. IV. The results are shown by the full lines in Fig. 7(a) and are seen to be in excellent agreement with the observed peak positions.

At $V_{\rm app}\sim1780$ mV, a sudden change in the form of the EL spectra is observed with the appearance of a number of more clearly resolved features. In addition, the slope of the variation of peak position with $V_{\rm app}$ is strongly reduced. The highest energy EL peak now consists of a pair of sharper peaks separated by $\sim$12 meV, the lower energy of which exhibits a number of GaAs LO$_\Gamma$ ($\sim$36 meV) phonon satellites. We identify these two peaks as X_{z1}-HH and $E_b(X_{z1})$, respectively. The slope of the peak position versus bias variation in Fig. 7(a) changes abruptly since the hot-electron population is now injected from an X-symmetry electronic state that is localized closer to the collector region at an energy below the emitter Fermi level (see Fig. 5).[24] In order to support this identification, the energy of the X_{z1}-HH transition was calculated as shown by the dashed line in Fig. 7. As for the $E_b(\Gamma)$ peak position calculated above, both the absolute energy and slope are very well described by the calculation; the change in the nature of the transport from nonresonant Γ-Γ tunneling to resonant Γ-X-Γ transfer is thus demonstrated. Very similar results were obtained for the 6-nm sample in Ref. 25, although in that case Γ-Γ features could only be observed over a very small bias range before the onset of Γ-X-Γ transfer.

For biases beyond the onset of Γ-X transfer, for the 4.5-nm sample, we could not detect any structured EL on the high-energy side of X_{z1}-HH. The absence of $E_b(\Gamma)$ is notable; at $V_{\rm app}\sim1860$ mV, for example, it is expected to arise at $\sim$40 meV to higher energy than X_{z1}-HH [see Fig. 7(a)]. This demonstrates clearly that the Γ-X-Γ channel dominates the electron transport for biases beyond the onset of Γ-X transfer ($\sim$1760 mV). An estimate of the upper limit for the relative strength of the two transport channels can be obtained by comparing the EL intensity of $E_b(X_{z1})$ with that of the high-energy tail of X_{z1}-HH under which $E_b(\Gamma)$ emission is concealed. From the EL spectra in Fig. 6, we estimate that the Γ-X-Γ transport channel is at least $\sim$500 times stronger than that for nonresonant Γ-Γ tunneling, for $V_{\rm app}$

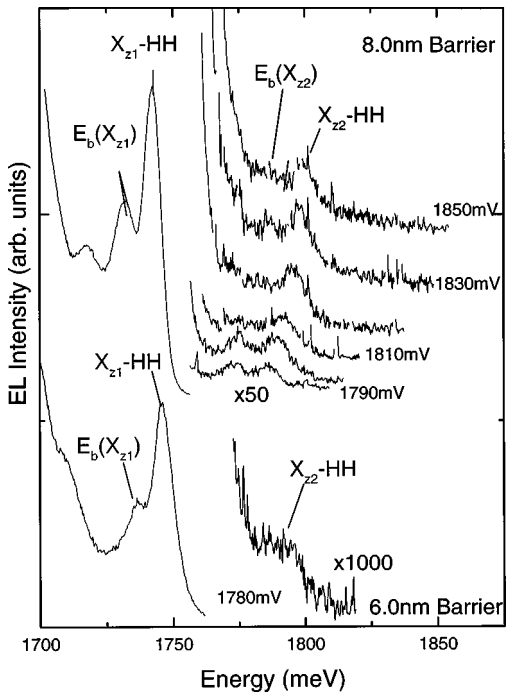

FIG. 8. Excited-state EL spectra obtained from 6-nm and 8-nm barrier samples for applied biases in excess of the onset of elastic Γ-X_{z2} transfer.

$=1860$ mV, and thus the electron Γ-X-Γ transport time ($\tau_{\Gamma X\Gamma}$) is at least $\sim$500 times faster than the nonresonant Γ-Γ tunneling time ($\tau_{\Gamma\Gamma}$).

VI. EXCITED-STATE ELECTROLUMINESCENCE

For biases beyond the onset of Γ-X_{z2} transfer, electrons transfer simultaneously into X_{z1}, X_{z2}, and X_{xy1} states, with the steady-state population of each being governed by the relative time scales over which intersubband ($X_{z2}\rightarrow X_{z1}$, $X_{z2}\rightarrow X_{xy1}$, and $X_{xy1}\rightarrow X_{z1}$) scattering and X-Γ (collector) transfer take place. Electrons populating excited X states will then generate type-II and hot-electron EL (Fig. 5) on the high-energy side of the ground-state type-II emission discussed in the previous section. Such excited-state EL provides quantitative information about energy relaxation within the AlAs barrier including the relative time scales over which intersubband and X-Γ scattering take place. A preliminary version of this work was presented in Ref. 26, but with very limited quantitative interpretation or discussion.

The 4.5-nm barrier sample is not expected to generate observable excited state EL in the present experiments since the onset of elastic Γ-X_{z2} transfer is calculated to be $V_{\rm app}\sim 2020$ mV, much higher than the biases investigated here. However, for wider barriers the onset of Γ-X_{z2} elastic transfer occurs at lower bias, and consequently excited-state EL features are expected, as shown in Fig. 8 for the 6- and 8-nm samples. The onset of elastic Γ-X_{z2} transfer arises at $V_{\rm app}\sim 1830$ mV and $V_{\rm app}\sim 1785$ mV for the 6- and 8-nm samples, respectively.

For the 6-nm sample, a weak shoulder is observed $\sim 45\pm 5$ meV to higher energy than X_{z1}-HH. This feature is approximately three orders of magnitude weaker than X_{z1}-HH and arises at an energy close to that expected for X_{z2}-HH recombination.[27] Much clearer excited-state emission is observed from the 8-nm sample, as seen in Fig. 8. Over the bias range 1790 mV$<V_{\rm app}<$1850 mV two weak peaks separated by $\sim$12 meV [labeled X_{z2}-HH and $E_b(X_{z2})$] are observed on the high-energy side of X_{z1}-HH. The bias dependence of the EL features is plotted in Fig. 7(b), with the full and dashed lines showing the calculated energies for X_{z1}-HH and X_{z2}-HH type-II emission, respectively. It is seen that excellent quantitative agreement is obtained between the calculated X_{z2}-HH positions and the experimental points. The lower-energy of the two peaks [$E_b(X_{z2})$] arises from e-A_0 recombination of ballistic electrons injected elastically into the collector from X_{z2}. The observed $\sim$12-meV energy separation is identical to that observed between X_{z1}-HH and $E_b(X_{z1})$ for the 4.5-nm barrier sample (see Sec. V).

Analysis of the relative intensities of both the $E_b(X_{z2})$:$E_b(X_{z1})$ and X_{z2}-HH:X_{z1}-HH peaks yields quantitative information regarding the relative population (n_2/n_1) and X-Γ lifetimes (τ_2/τ_1) of electrons populating the X_{z2} and X_{z1} states. The current density ($J_{1,2}$) injected into the collector from either X_{z1} or X_{z2} is given by

$$J_{1,2}=\frac{en_{1,2}}{\tau_{1,2}}. \tag{2}$$

The e-A^0 EL intensity arising from such monoenergetic hot electrons occupying conduction band states with kinetic energy E is given by[28] $I\propto J|M(E)|^2\tau_{\rm LO}$, where $|M(E)|^2$ is the energy-dependent e-A^0 recombination probability[29] and $\tau_{\rm LO}(E)$ is the GaAs LO phonon scattering time ($\sim$150 fs). Thus, the relative intensity of the $E_b(X_{z2})$ and $E_b(X_{z1})$ peaks [$I_b(X_{z1})/I_b(X_{z2})$] are related to the ratio J_1/J_2 via[30]

$$\frac{J_1}{J_2}=R\left(\frac{I_b(X_{z1})}{I_b(X_{z2})}\right), \tag{3}$$

where $R=|M(E_{z1})|^2/|M(E_{z2})|^2$. By combining Eqs. (2) and (3) we obtain

$$\frac{I_b(X_{z1})}{I_b(X_{z2})}\approx\frac{1}{R}\left(\frac{n_1}{n_2}\right)\left(\frac{\tau_2}{\tau_1}\right). \tag{4}$$

Thus, the relative intensities of the *ballistic* electron peaks arising from X_{z2} and X_{z1} is directly related to the product of the ratios of the X_z state X-Γ lifetimes and the steady-state level population ratios.

We now proceed by considering the relative intensities of the type-II EL peaks arising from the $X_{z2}[I_{\rm II}(X_{z2})]$ and $X_{z1}[I_{\rm II}(X_{z1})]$ states. This intensity ratio yields quantitative information about the population ratio of the X_{z2} and X_{z1} states (n_2/n_1) via the relation

$$\frac{I_{\rm II}(X_{z2})}{I_{\rm II}(X_{z1})}=\left(\frac{n_2}{n_1}\right)\left(\frac{|\langle X_{z2}|{\rm HH}_1\rangle|^2}{|\langle X_{z1}|{\rm HH}_1\rangle|^2}\right). \tag{5}$$

In Eq. (5), $|\langle X_{zi}|{\rm HH}\rangle|$ is the envelope function overlap between the ith X_z state and the confined $\rm HH_1$ state in the hole accumulation layer.

By fitting the hot electron and type-II EL peaks for the $V_{\rm app}=1790$ mV spectrum in Fig. 8, we measure $I_b(X_{z1})/I_b(X_{z2})=450\pm 30$ and $I_{\rm II}(X_{z1})/I_{\rm II}(X_{z2})=550\pm 50$. Correcting the latter value for the ratio of the envelope func-

tion overlaps ($\sim$0.93) we obtain $n_1/n_2 = 590 \pm 55$. By inserting this value into Eq. (5) we deduce $\tau_2/\tau_1 = 0.76 \pm 0.1$. Similar values are obtained for the other biases in Fig. 8.

This result demonstrates that the lifetimes of both the ground and first excited X_z state in the AlAs barrier are *comparable*, contrasting strongly with Γ-Γ-Γ resonant tunneling systems in which τ_2 is generally much shorter than τ_1. This arises since, for Γ-X-Γ resonant transport, there is no tunnel barrier impeding X(barrier)-Γ(collector) transfer. Thus, $\tau_{2,1}$ depends solely upon the intervalley X-Γ scattering time, which is expected to be only weakly dependent on the energy of the X_z state involved.

For biases in excess of the onset of Γ-X_{z2} transfer, emitter electrons transfer principally into the X_{z2} state since the Γ-X_{z1} coupling is much weaker. Despite this, the excited-state EL features in Fig. 8 remain much weaker than the corresponding X_{z1}-related hot-electron and type-II features. This demonstrates clearly that the complete Γ-X-Γ transport process is *very* strongly sequential in nature with Γ(emitter)-X(barrier) transfer occurring first, followed by relaxation within the AlAs barrier, before X(barrier)-Γ(collector) transfer takes place.

In order to clarify quantitatively the sequential nature of the Γ-X-Γ transport, we estimated the relative magnitude of the X_{z2}-X_{z1} scattering time (τ_i) and the X-Γ transfer time for electrons populating X_{z2} (τ_2). Assuming that electrons transferring into X_{z2} either scatter to X_{z1} or undergo intervalley X-Γ(collector) transfer[31] we may write

$$\frac{\tau_i}{\tau_2} = \left\{ \frac{\tau_2}{\tau_1}\frac{n_1}{n_2} - 1 \right\}^{-1}. \tag{6}$$

Inserting the values of (n_1/n_2) and (τ_2/τ_1) determined above into Eq. (6), we determine $(\tau_i/\tau_2) = 2 \pm 0.5 \times 10^{-2}$ thus demonstrating clearly that the Γ-X-Γ transport process is very strongly sequential.

VII. Γ-X-Γ AND Γ-Γ TUNNELING TIMES

In this section we consolidate some of our principal findings by comparing the Γ-X-Γ transport time ($\tau_{\Gamma\text{-}X\text{-}\Gamma}$) deduced from the σ-V modeling in Sec. IV and the EL results presented above, with that expected for nonresonant Γ-Γ transport ($\tau_{\Gamma\Gamma}$) through the AlAs barrier. We calculate $\tau_{\Gamma\Gamma}$ using a WKB representation for the tunneling probability, combined with a semiclassical tunneling attempt rate calculated using the self-consistent Poisson-Schrödinger modeling described earlier. For the calculation, we use $\sim$910 meV for the conduction-band offset at the GaAs-AlAs heterointerface, together with Γ-point electron effective masses of $0.068m_0$ and $0.1m_0$ for GaAs and AlAs, respectively. The Γ-X-Γ transport time ($\tau_{\Gamma\text{-}X\text{-}\Gamma}$) calculated represents the value *averaged* over the emitter distribution.

Figure 9 shows the results of the calculations as a function of the electric field in the AlAs barrier (40–200 kV/cm) for barrier widths between 3.0 and 10 nm. The calculated variations of ($\tau_{\Gamma\text{-}X\text{-}\Gamma}$) and $\tau_{\Gamma\Gamma}$ with electric field are shown by the curves with and without symbols, respectively. The arrows mark the fields at which Γ-X transfer commences for each barrier width.

We find that the calculated value of $\tau_{\Gamma\text{-}X\text{-}\Gamma}$ close to the onset of Γ-X transfer increases strongly with the AlAs barrier width. This behavior reflects primarily the decrease of the Γ-X coupling strength [Eq. (1)] as the Γ and X envelope functions become more spatially separated in wider barrier structures. However, for electric fields significantly beyond the onset of Γ-X transfer (>150 kV/cm) $\tau_{\Gamma\text{-}X\text{-}\Gamma}$ is observed to saturate at a value between $\sim$0.1 and 1 ns for *all* barrier widths. This behavior arises from a balance between two competing effects: first, as the width of the AlAs barrier decreases, the strength of the Γ-X coupling *per X state* increases. This effect alone would result in a pronounced strengthening of the role of Γ-X-Γ transport for smaller AlAs barrier widths. However, for thinner AlAs barriers quantum confinement effects become more pronounced with the result that the average energy spacing between X states increases. This reduces the total number of X states available for conduction at a fixed electric field and results in an overall weakening of the contribution from the Γ-X-Γ transport channel. The calculation indicates that these two opposing effects partially compensate each other, with the result that for electric fields (biases) beyond the onset of Γ-X-Γ transfer, $\tau_{\Gamma\text{-}X\text{-}\Gamma}$ becomes only *weakly* dependent upon the barrier width. The occurrence of such saturation behavior for $\tau_{\Gamma\text{-}X\text{-}\Gamma}$ with electric field permits us to state that for AlAs barrier widths greater than $d \sim 3.0$ nm Γ-X-Γ processes dominate *whenever* intervalley Γ-X transfer is energetically possible whereas for $d < 2.5$ nm nonresonant Γ-Γ tunneling will dominate the electron transport characteristics. The results of Fig. 9 are in good agreement with our experimental findings; in Sec. IV and Ref. 4, where we found that Γ-X-Γ transport dominates for all samples investigated ($d = 4.5$–10 nm) whenever energetically possible. Furthermore, for the 4.5-nm sample we estimated ($\tau_{\Gamma\text{-}\Gamma}/\tau_{\Gamma\text{-}X\text{-}\Gamma}$) $\sim$500 in Sec. V from the absence of $E_b(\Gamma)$ for biases above the threshold for intervalley Γ-X-Γ transfer. This observation is in good agreement with the calculated ($\tau_{\Gamma\text{-}\Gamma}/\tau_{\Gamma\text{-}X\text{-}\Gamma}$) $= 200 \pm 50$ at 170 kV/cm. We note, however, that further quantitative comparison of the calculations of $\tau_{\Gamma\Gamma}$ in Fig. 9 with, for example, the nonresonant Γ-Γ tunnel current flowing for biases below the onset of Γ-X transfer (Fig. 3) is difficult since leakage currents

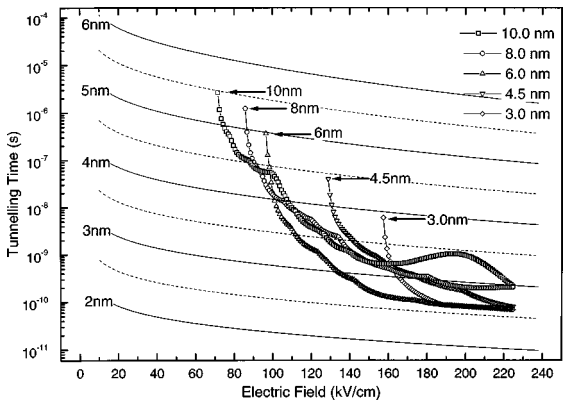

FIG. 9. Calculated Γ-Γ tunneling times (full lines 2, 3, 4, 5, and 6 nm, dashed lines 2.5, 3.5, 4.5, and 5.5 nm) and Γ-X-Γ (symbols) transfer times through single AlAs barrier as the electric field and width of the barrier is varied. The value of $\tau_\Gamma X_\Gamma$ presented represents an average over the emitter distribution.

may contribute significantly to the total tunnel current at lower biases.

VIII. CONCLUSIONS

In summary, we have combined electrical transport measurements with sensitive EL spectroscopy techniques to investigate the comparative roles of nonresonant Γ-Γ and intervalley Γ-X-Γ transport process through indirect-gap GaAs-AlAs-GaAs single-barrier structures. The contribution to the total current from Γ-Γ tunneling was shown to be very small for AlAs barrier widths greater than 4.5 nm, with Γ-X-Γ intervalley transport dominating *whenever* energetically possible.

The Γ-X-Γ transport process has been shown to take place predominantly without conservation of the transverse wave vector ($k_{\|}$), an effect that arises from the differing effective masses of the Γ (emitter) and X (barrier) electronic states. Sharply peaked structure observed in the conductance-voltage characteristics of thinner barrier structures close to the onset of Γ-X transfer was shown to be consistent with a weak $k_{\|}$ conserving contribution to the Γ-X-Γ transport, which had been assumed to dominate the Γ-X-Γ transport process in much previous work. By detecting extremely weak EL emission arising from excited X states within the AlAs barrier, the entire Γ-X-Γ tunneling process was shown to be *very* strongly sequential with Γ-X scattering occurring first, followed by carrier relaxation within the X valley of AlAs, before X-Γ transfer occurs. In addition, the comparative X-Γ lifetimes of the X_{z2} and X_{z1} states were shown to be similar.

Finally, application of a $k_{\|}$ nonconserving model for the Γ-X intervalley transfer process enabled us to determine quantitative values for the Γ-X-Γ transport time and its dependence upon both the width and the electric field in the AlAs barrier. From these calculations, we showed that nonresonant Γ-Γ tunneling is only important for barrier widths less than ~3 nm or when Γ-X intervalley scattering is not energetically allowed.

*Present address: Walter Schottky Institut, Am Coulombwall, D-85748 Garching, Germany.

[1] E. E. Mendez, E. Calleja, C. E. T. Gonçalves da Silva, L. L. Chang, and W. I. Wang, Phys. Rev. B **33**, 7368 (1986).

[2] S. Adachi, J. Appl. Phys. **58**, R1 (1985).

[3] D. Bimberg, W. Bludau, R. Linnebach, and E. Bauser, Solid State Commun. **37**, 987 (1981).

[4] R. Teissier, J. J. Finley, M. S. Skolnick, J. W. Cockburn, J. L. Pelouard, R. Grey, G. Hill, M. A. Pate, and R. Planel, Phys. Rev. B **54**, R8329 (1996).

[5] A. R. Bonnefoi, L. F. Luo, W. I. Wang, and E. E. Mendez, Phys. Rev. B **37**, 8754 (1988).

[6] R. Beresford, L. F. Luo, W. I. Wang, and E. E. Mendez, Appl. Phys. Lett. **55**, 1555 (1989).

[7] H. C. Liu, Appl. Phys. Lett. **51**, 1019 (1987).

[8] E. L. Ivchenko, A. A. Kiselev, Y. Fu, and M. Willander, Phys. Rev. B **50**, 7747 (1994).

[9] T. Ando, S. Wakahara, and H. Akera, Phys. Rev. B **40**, 11 609 (1989); **40**, 11 619 (1989).

[10] The conduction-band ellipsoids are characterized by transverse (m_{Xxy}) and longitudinal (m_{Xz}) effective masses of $0.26m_0$ and $0.84m_0$, respectively.

[11] H. W. van Kesteren, E. C. Cosman, P. Dawson, K. J. Moore, and C. T. Foxon, Phys. Rev. B **39**, 13 426 (1989).

[12] P. Dawson, C. T. Foxon, and H. W. van Kesteren, Semicond. Sci. Technol. **5**, 54 (1990).

[13] J. Feldmann, J. Nunnenkamp, G. Peter, E. Göbel, J. Kuhl, K. Ploog, P. Dawson, and C. T. Foxon, Phys. Rev. B **42**, 5809 (1990).

[14] H. Ohno, E. E. Mendez, and W. I. Wang, Appl. Phys. Lett. **56**, 1793 (1990).

[15] For all samples investigated in the present work, the Γ-Γ-Γ tunneling current is dominated by electron transport with holes providing a much smaller contribution. This arises as a consequence of the much larger hole effective mass ($m_h^* = 0.34m_0$) in GaAs than for electrons ($m_e^* = 0.067m_0$).

[16] L. Eaves, G. A. Toombs, F. W. Sheard, C. A. Payling, M. L. Leadbeater, E. S. Alves, T. Foster, P. E. Simmonds, M. Henini, O. S. Hughes, J. C. Portal, G. Hill, and M. A. Pate, Appl. Phys. Lett. **52**, 212 (1987).

[17] J. J. Finley, R. J. Teissier, M. S. Skolnick, J. W. Cockburn, R. Grey, G. Hill, and M. A. Pate, Phys. Rev. B **54**, R5251 (1996).

[18] An identical situation exists for the case of Γ-Γ-Γ resonant tunneling systems where in general $\Delta k_{\|} = 0$ elastic tunneling dominates the transfer process since more emitter electrons can participate at a single bias.

[19] C. L. Petersen, M. R. Frei, and S. A. Lyon, Phys. Rev. Lett. **63**, 2849 (1989).

[20] D. N. Mirlin, V. F. Sapega, I. Ya Karlik, and R. Katilius, Solid State Commun. **61**, 799 (1987).

[21] R. Teissier, J. J. Finley, M. S. Skolnick, J. W. Cockburn, R. Grey, G. Hill, and M. A. Pate, Phys. Rev. B **51**, 5562 (1995).

[22] P. Dawson, C. T. Foxon, and H. W. van Kesteren, Semicond. Sci. Technol. **5**, 54 (1990).

[23] As expected for such a hot electron distribution, the linewidth (FWHM) of $E_b(\Gamma)$ increases from ~20 to 35 meV as the applied bias is increased from 1640 to 1730 mV. This reflects primarily the increase of Fermi energy of the emitter distribution with applied bias. Similar effects are observed in the hot electron EL spectra observed for $Al_xGa_{1-x}As$ direct gap tunneling diodes, as discussed in Ref. 21.

[24] The sharpening of the EL spectra at the transition (V_t) from Γ-Γ to Γ-X-Γ transport arises since, below V_t, electrons are injected into the collector from the emitter distribution, which has a large Fermi energy (~30–50 meV). Above V_t, electrons are injected from the X state in the barrier where the Fermi energy is expected to be much lower (≤1 meV).

[25] J. J. Finley, R. J. Teissier, M. S. Skolnick, J. W. Cockburn, R. Grey, G. Hill, and M. A. Pate, Surf. Sci. **362**, 197 (1996).

[26] J. J. Finley, J. W. Cockburn, M. S. Skolnick, R. Grey, G. Hill, M. A. Pate, and R. Teissier, in *Proceedings of the 23rd International Conference on the Physics of Semiconductors, Berlin 1996*, edited by M. Scheffler and R. Zimmermann (World Scientific, Singapore, 1996), p. 2255.

[27] We calculate $E(X_{z2} - X_{z1}) \sim 38.5$ meV for $V_{app} = 1820$ mV.

[28] R. Teissier, J. W. Cockburn, P. D. Buckle, M. S. Skolnick, J. J.

Finley, R. Grey, G. Hill, and M. A. Pate, Phys. Rev. B **50**, 4885 (1994).

[29] W. P. Dumke, Phys. Rev. **132**, 1998 (1963).

[30] Since τ_{LO} is only weakly energy dependent for $E_c \gg \hbar\Omega_{\mathrm{LO}}$—see W. Fawcett, A. D. Boardman, and S. Swain, J. Phys. Chem. Solids **31**, 1963 (1970).

[31] For the 8-nm barrier sample, we calculate that the energy separation between X_{z2} and X_{z1} is 47–52 meV for the bias range over which excited state emission is observed (1780–1850 meV). This is very close to the Γ-point LO phonon energy in AlAs enabling intersubband scattering to be mediated by zone center LO phonon emission. Such intersubband scattering by small wave-vector phonons is expected to be very fast, proceeding over typical time scales of several hundred femtoseconds [R. Ferreira and G. Bastard, Phys. Rev. B **40**, 1074 (1989)]; By contrast, $X_{z2}-X_{xy1}$ inequivalent intervalley scattering requires the participation of large-wave-vector acoustic and optical phonons and is expected to take place over time scales longer than a picosecond [S. Zollner, S. Gopalan, and M. Cardona, J. Appl. Phys. **68**, 1682 (1990)]. Thus, electrons transferring into X_z states are expected to remain in the longitudinal X states until X-Γ transfer occurs.